Effect of spinel and perovskite coatings on the long term oxidation of a ferritic stainless steel in H2/H2O atmosphere

M.R. Ardigo-Besnard, I. Popa, S. Chevalier

Effect of spinel and perovskite coatings on the long term oxidation of a ferritic stainless steel in H_2/H_2O atmosphere

M. R. Ardigo-Besnard[1], I. Popa, S. Chevalier

Laboratoire Interdisciplinaire Carnot de Bourgogne (ICB), UMR 6303 CNRS, Univ. Bourgogne Franche-Comté, BP 47870, 21078 DIJON Cedex, France

Abstract

In order to improve the oxidation behaviour of AISI441 ferritic stainless steel in H_2/H_2O atmosphere at 800°C, four oxide coatings were tested: two perovskites ($La_{0.8}Sr_{0.2}MnO_3$ and $LaNi_{0.6}Fe_{0.4}O_3$) deposited by screen printing and two spinels ($MnCo_2O_4$ and Co_3O_4) obtained by PVD technique. Isothermal oxidation tests performed up to 3000 hours showed that the coating presence avoided Fe oxides growth, which occurs for the raw alloy in the same conditions. Moreover, a protective $(Cr,Mn)_3O_4/Cr_2O_3$ layer formed between the substrate and the coating. Any presence of Cr was not detected within the coatings, indicating that all compositions were efficient in preventing Cr evaporation.

Keywords: stainless steel, oxidation, high temperature corrosion, oxide coatings, SEM, X-ray diffraction

[1] Corresponding author. Tel.: +33 (0)380396016; fax: +33 (0)380396132.
E-mail address: maria-rosa.ardigo-besnard@u-bourgogne.fr

1. Introduction

Ferritic stainless steels are widely used at high temperature in aggressive atmospheres, such as water vapour enriched, because of their considerable corrosion resistance [1,2]. Previous studies [3,4] were carried out on K41X stainless steel (AISI 441) in O_2/H_2O and H_2/H_2O atmospheres at 800°C for fuel cell application. In O_2/H_2O atmosphere [3] the corrosion scale is formed by an inner Cr_2O_3 layer and an outer $(Cr,Mn)_3O_4$ spinel-type oxide. For long-time exposure, the evaporation of chromium species occurs from $(Cr,Mn)_3O_4$ spinel phase, as well as from any Cr_2O_3 that is not covered by the spinel layer. This phenomenon may cause a depletion of chromium content in the alloy, inducing a reduction of the protective properties of the steel [5]. Oxidation tests performed in H_2/H_2O atmosphere up to 3000 hours revealed that a non-protective Fe_3O_4 layer grew on top of an inner $(Cr,Fe)_2O_3$ oxide. It was shown that the formation of this non-protective double scale strictly depends on the alloy surface finishing [4].

In order to improve the oxidation behaviour in both O_2/H_2O and H_2/H_2O atmospheres, the alloy can be surface-modified via the application of coatings, as an alternative approach to bulk composition modification. These coatings are intended to serve as barrier to Cr and Fe outward diffusion and O inward diffusion. In O_2/H_2O atmosphere, they should reduce the growth kinetics of chromia Cr_2O_3 and inhibit Cr migration from Cr-rich oxide scales or Cr-containing substrate [6]. On the other hand, in H_2/H_2O atmosphere, they should protect against the growth of non-protective Fe-rich oxides, such as $(Cr,Fe)_2O_3$ and Fe_3O_4. Moreover, coatings should improve the oxide scale adhesion to the metallic substrate [7].

Coatings developed so far can be of four types [8]: reactive element oxides, MAlCrYO (M = transition metal) oxidation resistant systems, conductive perovskites and spinel-type oxides. Although coatings of reactive element oxides have demonstrated to significantly enhance

scale adhesion and reduce the oxidation rate [9-15], they may not be effective at inhibiting Cr diffusion and preventing Cr evaporation [8].

Rare earth perovskite coatings are interesting as they have compatible thermal expansion coefficient with the ferritic substrate and supply reactive elements to the underlying growing oxide scale, improving the oxidation behaviour [8,16,17]. They allow to decrease the oxidation rate and to enhance the oxide scale adhesion [18-27]. However, because of their ionic conductive nature, perovskites are not suitable for protection purposes as they may transport oxygen ions and do not substantially inhibit Cr migration or adsorb Cr migrating species [18]. Moreover, the high sintering temperature of perovskites, does not allow obtaining fully dense layers [8].

Nevertheless, literature data show that the addition of $La_{1-x}Sr_xMnO_{3-\delta}$ coating (with $0.1 \leq x \leq 0.33$) limits the evaporation of chromium species, as volatile Cr (VI) species easily react with Mn present in the coating and form $(Cr,Mn)_3O_4$ phase. However, the substrate oxidation is not completely avoided [28,29].

The best results against Cr evaporation were achieved with $LaNi_{0.6}Fe_{0.4}O_{3-\delta}$ coating, that significantly inhibits the deposition of Cr species as compared to LSM [17,30].

In parallel, spinel oxides show excellent capability for blocking outward Cr diffusion. The compositions Co_3O_4, $CuFe_2O_4$, $Mn_xCo_{3-x}O_4$, $Cu_xMn_{3-x}O_4$ (where $1 \leq x \leq 1.5$) present the best thermal expansion coefficient match with the ferritic steel [7]. Mn-containing spinels are the easiest to sinter [7]. Mn-Co spinels were widely studied in literature and were found to show good protection against oxidation in air at high temperature [31-33], to have excellent capability for blocking outward Cr diffusion [6,34-36] and good compatibility (mechanical and chemical) with the bcc ferritic steel substrate [37].

All these oxides were largely studied for application as protective coating at high temperature in air. However, literature contains very little information describing the coatings behaviour in

reducing atmosphere [15,38]. Generally speaking, a coating under H_2 atmosphere would not be needed, as the low oxygen partial pressure results in negligible Cr evaporation rates [39-41]. However, even if Cr evaporation is not an issue, in order to use K41X as-rolled alloy in H_2/H_2O atmosphere, a coating is needed in order to protect against the growth of Fe oxides.

Based on the literature data presented here above, in the present study four coatings were chosen and tested: $La_{0.8}Sr_{0.2}MnO_3$ (LSM) and $LaNi_{0.6}Fe_{0.4}O_3$ (LNF) perovskites; $MnCo_2O_4$ and Co_3O_4 spinels. LSM and LNF were deposited by screen printing and $MnCo_2O_4$ and Co_3O_4 by PVD technique. The K41X coated samples were tested under 10 % H_2 - 90 % H_2O atmosphere at 800°C up to 3000 hours. The effect of the chosen coatings on long term high temperature oxidation behaviour of K41X as-rolled alloy was investigated by scanning electron microscopy (SEM) and X-ray diffraction (XRD) analyses performed before and after ageing tests.

2. Materials and methods

The alloy tested in the present study is a commercial stainless steel, K41X (AISI 441), with a chromium content of 18 wt. % (Fe – 18 % Cr - 0.58 % Si - 0.52 % Nb - 0.25 % Mn - 0.14 % Ti). The size of the samples was 20 mm x 20 mm and 1 mm thick.

$La_{0.8}Sr_{0.2}MnO_3$ (LSM) and $LaNi_{0.6}Fe_{0.4}O_3$ (LNF) coatings were deposited by screen printing process. Slurries were prepared by dispersion of LSM or LNF powder in a solution containing 5 wt. % of ethyl cellulose in terpineol. The adhesion and the density of the coatings were improved by a thermal treatment of 5 hours at 850°C in air.

$MnCo_2O_4$ and Co_3O_4 coatings were deposited on the steel surface by physical vapour deposition (PVD). Co_3O_4 was directly obtained by reactive magnetron sputtering, followed by 10 hours crystallisation treatment in air at 800°C. For $MnCo_2O_4$ coating, metallic Co and Mn

were co-sputtered on the steel surface; 10 hours oxidation treatment in air at 800°C was then carried out, in order to obtain the desired oxide stoichiometry, $MnCo_2O_4$.

All the coatings present significant thicknesses (between 4 and 20 µm), in order to provide an effective barrier against the diffusion of chemical species.

Ageing tests were carried out at 800°C up to 3000 hours in a horizontal furnace. For safety reasons, H_2 was diluted into Ar and the real gas composition used during isothermal oxidation experiments was Ar - 1 % H_2 - 9 % H_2O. The oxygen partial pressure corresponding to this atmosphere is of 10^{-16} bar. More details about the experimental device can be found elsewhere [5,42].

Before and after oxidation tests, the coated samples (surfaces and cross-sections) were carefully characterised using scanning electron microscopy (JEOL JSM-7600F) coupled with energy dispersive X-ray spectrometry (Oxford LINK EXLII). In parallel, X-ray diffraction (XRD) analyses were performed at fixed incidence angle of 8° with INEL CPS 120 diffractometer using Cu Kα (λ = 0.154056 nm) radiation.

3. Results and discussion

Figure 1 presents the surface weight change of K41X coated samples after 200, 1000 and 3000 hours ageing at 800°C in H_2/H_2O atmosphere, as compared to values obtained for the uncoated samples. The coating presence allows improving the oxidation behaviour, with weight changes that strongly diminish for all the coated samples and this for all considered exposure periods. As it will be discussed in details in the following paragraphs, this improvement could be related to the fact that Fe oxides growth could be avoided during high temperature oxidation; instead, the formation of continuous thin layers of $(Cr,Mn)_3O_4/Cr_2O_3$ between the metallic substrate and the coating was observed in all cases.

3.1 LSM coated K41X samples

Figure 2 (a) and (b) show SEM surface and cross-section micrographs of LSM coated K41X as-rolled alloy after annealing for 5 hours at 850°C in air. The expected $La_{0.8}Sr_{0.2}MnO_3$ stoichiometry has a La/Sr ratio of 4. The LSM coating of about 11 µm thickness is a single-phase with a La/Sr ratio of 5, corresponding to $La_{0.84}Sr_{0.16}MnO_3$ composition. Some porosity can be noticed, because of incomplete sintering (a porosity of less than 20 % is considered as acceptable) or issued from the thermal expansion coefficient difference between LSM and the K41X stainless steel (of $11.6 \cdot 10^{-6}$ K^{-1} [16] and $12.2 \cdot 10^{-6}$ K^{-1} [17] respectively, at 800°C). Nevertheless, any significant oxidation of the metallic substrate did not occur during the annealing step, probably because of the rather significant thickness of the coating.

After oxidation tests for 200 and 3000 hours ageing at 800°C in H_2/H_2O atmosphere, the surface and cross-section microstructures of LSM coated K41X samples are presented in Fig. 2 (c)-(f). A duplex $(Cr,Mn)_3O_4/Cr_2O_3$ oxide scale formed between the coating and the steel substrate. Its thickness is less than 1 µm after 200 hours (Fig. 2 (d)) and it does not exceed 1.5 µm after 3000 hours of exposure (Fig. 2 (f)). Any significant degradation of LSM coating with the exposure time was not found (the crack present in Fig. 2 (f), parallel to the interface between LSM coating and the duplex oxide scale is due to cross-section preparation).

After 200 hours of thermal treatment, the presence of a very small amount of MnO was evidenced by XRD analyses. After 3000 hours of exposure, EDX analyses revealed that the LSM stoichiometry was modified. SEM elementary mapping (Fig. 3) showed that some Mn-rich oxide nodules (MnO as confirmed by XRD) were dispersed randomly over the upper two-thirds of the coating. Moreover, a non-continuous MnO layer of about 1 µm thickness formed at the interface between the coating and the duplex $(Cr,Mn)_3O_4/Cr_2O_3$ layer.

The MnO appearance can be related to a partial LSM decomposition that was shown by several works to take place under low oxygen partial pressure, below 10^{-12} bar [27,43] and

that in the present study occurs from 200 hours of exposure. A two-steps mechanism can be suggested:

- in a first time, Cr-Mn spinel should form by reaction between chromia and LSM perovskite. This suggestion is in agreement with literature observations mentioning that manganese-containing perovskites, particularly LSM, facilitate the formation of manganese-containing spinels, like $(Mn,Cr)_3O_4$, through reactions between the oxide scale and the manganite perovskites [45-47];
- subsequently, the non-continuous MnO layer should form by reaction between Mn, coming from $(Cr,Mn)_3O_4$, and O diffusing through the porous LSM coating. This hypothesis is in agreement with the observations of Zhen et al. [48] who consider that Mn source is $(Cr,Mn)_3O_4$.

In parallel, it can also be supposed that MnO formation follows an outward diffusion of Mn coming from substrate and an inward O diffusion through the porous LSM layer (in agreement with the higher diffusivity of Mn in reducing atmosphere [44]). This idea is supported by Mn depletion at the inner part of the coating (16 at. % instead of 20 at. %) and Mn increased content at the outer part (24 at. % instead of 20 at. %) after 3000 hours of exposure.

~~Based on this supposed two-step mechanism, MnO formation involves $(Cr,Mn)_3O_4$ decomposition, explaining why the thickness of the $(Cr,Mn)_3O_4/Cr_2O_3$ duplex layer does not increase significantly from 200 up to 3000 hours of exposure.~~

~~Taking into account all these considerations, it is possible to suggest that, even if $(Cr,Mn)_3O_4$ phase is immediately transformed in MnO for short exposure time, the mass increase of the LSM-coated K41X samples is mainly related to the growth and thickening in time of the duplex $(Cr,Mn)_3O_4/Cr_2O_3$ oxide layer at the interface between the LSM layer and the stainless steel. On the other hand, for long exposure time, the higher presence of MnO phase inside the~~

~~coating and at the interface between the coating and the duplex $(Cr,Mn)_3O_4/Cr_2O_3$ layer also significantly contributes to the weight gain, explaining the important increase observed after 1000 hours of thermal treatment (Fig. 1).~~

~~The presence of a fine and non-continuous SiO_2 layer at the $(Cr,Mn)_3O_4/Cr_2O_3$ duplex oxide scale/metal substrate interface can be observed in Fig. 3 after 3000 hours ageing. MEB-EDX analyses revealed that this non-continuous SiO_2 layer formed from the first exposure instants in H_2/H_2O atmosphere and did not significantly evolve with the exposure time.~~

~~Moreover, for all ageing times, TiO_2 precipitates were detected beneath the SiO_2 layer, according to the Ellingham-Richardson diagram [49] (the oxygen partial pressures needed for TiO_2 et SiO_2 formation are 10^{-36} et 10^{-33} bar respectively).~~

After 3000 hours ageing, some Sr segregation at the coating surface was shown by cross-section EDX elementary mapping (Fig. 3). Indeed, La/Sr ratio of the coating decreased to 3.5 from the initial value of 5. This behaviour is in agreement with the observations of Caillol et al. [50] after $La_{0.8}Sr_{0.2}MnO_3$ annealing at low oxygen pressures (1% O_2 - 99% N_2) at 900°C. A similar result was found after heating a $La_{0.5}Sr_{0.5}MnO_3$ sample under UHV (10^{-6} mbar oxygen partial pressure) at 600°C; the formation of SrO was found in this case [51]. As it was reviewed by Jiang [16], Sr outward migration occurs for other La-Sr based perovskites at high temperatures, low oxygen pressures and under polarisation. The intrinsic segregation of Sr was explained to be strain driven because of the ionic radius of Sr^{2+} dopant that is larger than of the La^{3+} host. The dopant will produce then less elastic strain when it is present at the surface than in the bulk sites. Jiang [16] suggests that the Sr-enriched regions are most likely SrO, since Sr does not exist in a free state.

Some spalling can be noticed at the LSM surface after thermal treatment (Fig. 2 (c) and (e)), probably in relation with the elastic strain mentioned here above. The phenomenon increases

after 3000 hours, which suggests that at least another cause might be responsible, probably the Sr segregation as SrO.

In consequence, the mass increase of LSM coated K41X samples is mainly related to MnO and Cr_2O_3 layers that present an increasing thickness with the ageing time. Moreover, the mass increase can equally be explained by the presence of a fine and non-continuous SiO_2 layer at the $(Cr,Mn)_3O_4/Cr_2O_3$ duplex oxide scale/metallic substrate interface that can be observed in Fig. 3 after 3000 hours ageing. In addition, TiO_2 precipitates were detected at the outer part of the steel beneath the SiO_2 layer, in agreement with Ellingham-Richardson diagram [49] (the oxygen partial pressures needed for TiO_2 et SiO_2 formation are of 10^{-36} et 10^{-33} bar respectively).

~~Any Cr diffusion into LSM coating was not observed in H_2-H_2O atmosphere, probably because the continuous formation of $(Cr,Mn)_3O_4$ phase that is immediately transformed in MnO. This latter layer seems to be efficient in blocking Cr outward diffusion.~~

Contrarily to oxidising atmospheres, Cr evaporation is not an issue in H_2-H_2O atmospheres. Indeed, the low oxygen partial pressure of 10^{-16} mbar, corresponding to Ar - 1 % H_2 - 9 % H_2O environment of this study, results in negligible rates of Cr evaporation [39-41]. In agreement, any Cr diffusion was not observed into LSM coating in H_2-H_2O atmosphere. The continuous formation of $(Cr,Mn)_3O_4$ phase should equally have a positive impact in blocking Cr outward diffusion. This observation is in agreement with the studies of Yang et al. [45] showing that the presence of LSM coating avoids Cr diffusion with further formation of $SrCrO_4$, contrarily to $La_{0.8}Sr_{0.2}CoO_3$ coating, the reason being the presence of $(Cr,Mn)_3O_4$ layer. However, even if $SrCrO_4$ phase is avoided in oxidising atmosphere, Cr enrichment of LSM layer can take place if a good densification is not reached [52] or in presence of water vapour [53]. Preoxidation of the stainless steel in order to increase the proportion of

$(Cr,Mn)_3O_4$ scale relative to Cr_2O_3 was then performed and showed a decrease of Cr diffusion phenomena [54,55].

After thermal ageing of LSM coated stainless steels in oxidising atmospheres, most of the authors show that Cr deposition takes place through the whole thickness of the coating, but decreases with the distance from the alloy surface [48,52,53]. Much less studies report that Cr migration is avoided [45]. It is however the case in the present study after exposure in H_2-H_2O atmosphere; indeed, after 3000 hours, any presence of Cr was not observed inside the coating layer. However, a Fe enrichment, of about 8 at. % was measured. This kind of phenomena does not occur during air exposition, even in presence of a high level of moisture [53]. At most, some Fe enrichment of $(Cr,Mn)_3O_4$ spinel was only reported [29,56]. It can be supposed that Fe mobility is enhanced by the presence of H_2, as it was previously observed for the uncoated as-rolled alloy [4]. Moreover, Fe has a coefficient of diffusion through chromia layers higher than Mn and Cr [57]. In the present study, the thickness of the duplex $(Cr,Mn)_3O_4/Cr_2O_3$ layer is rather low (about 1.5 µm after 3000 hours ageing) and the LSM coating is not fully densified. It results that in H_2/H_2O atmosphere, Fe can easily diffuse from the stainless steel through the rather thin $(Cr,Mn)_3O_4/Cr_2O_3$ layer and enrich the whole thickness of the porous LSM coating.

3.2 LNF coated K41X samples

SEM surface and cross-section images of LNF coated K41X sample as annealed in air at 850°C for 5 hours are showed in Fig. 4 (a) and (b). EDX analyses confirmed that the coating presented the expected $LaNi_{0.6}Fe_{0.4}O_3$ composition. However, XRD patterns revealed a mixture of orthorhombic and rhombohedral LNF phases with some NiO traces. The single rhombohedral $LaNi_{0.6}Fe_{0.4}O_3$ was not reached, probably because of a too short annealing

treatment or too low temperature; indeed Basu et al. [17] obtained the single $LaNi_{0.6}Fe_{0.4}O_3$ phase after 5 hours at 900°C, but after the same time at 800°C a certain amount of orthorhombic phase is equally present. Even if some porosity can be observed, the significant thickness of LNF layer (of about 20 µm) limited the oxidation of the metallic substrate. Only a very thin Cr_2O_3 layer formed at the interface with the metal (Fig. 4 (b)).

After thermal ageing in H_2/H_2O atmosphere, the LNF coated K41X samples present a small negative mass variation for exposure periods shorter than 1000 hours. As shown by SEM-EDX elementary mapping (Fig. 5) coupled with XRD analyses, the weight loss can be explained by LNF decomposition, leading to the appearance of metallic Ni that segregates mainly at the outer part of the coating, of a new LNF rhombohedral perovskite with different stoichiometry and of La_2O_3 phase (Fig. 4 (d)). ~~The decomposition of the LNF coating takes place from the first exposure instants; then the coating composition does not evolve and the same phases were detected for all exposure times, up to 3000 hours ageing (Fig. 4(f)).~~ NiO phase present in the initial coating composition was reduced to metallic Ni during the ageing treatment, as the oxygen partial pressure needed to stabilise NiO is of 10^{-14} bar, higher than the one available in Ar - 1 % H_2 - 9 % H_2O atmosphere. The corresponding value for La_2O_3 is of around 10^{-47} bar, while for the different Fe oxides, it is below 10^{-18} bar. XRD patterns registered at fixed angle indicated that La_2O_3 phase segregates at the inner part of the coating, as the corresponding peaks become lower with the exposure time. The decomposition of LNF coating takes place from the first exposure instants; then the coating composition does not evolve and the same phases were detected for all exposure times, up to 3000 hours ageing (Fig. 4(f)). ~~Compared to the LSM coating, a less important spalling can be observed at the LNF surface after thermal treatment in H_2/H_2O (Fig. 4 (c) and (e)).~~

At the interface between LNF coating and the metallic substrate, a $(Cr,Mn)_3O_4/Cr_2O_3$ duplex layer grows from the first exposure hours and slowly thickens with ageing time. Indeed, after

200 hours, the thickness of $(Cr,Mn)_3O_4/Cr_2O_3$ scale is less than 1 µm (Fig. 4 (d)) and does not overcome 2 µm after 3000 hours (Fig. 4 (f)). For this reason, a small mass uptake was measured after 3000 hours (Fig.1), while the coating composition did not evolve as compared to that obtained after 1000 hours ageing. However, $(Cr,Mn)_3O_4$ proportion is very low, in agreement with the literature showing that the formation of this phase is limited in presence of LNF coatings [58,59]. Some Cr (2 at. %) was detected all over the thickness of the coating, indicating that LNF coating used in this study is able to limit Cr outward diffusion, but not completely block it.

~~At the $(Cr,Mn)_3O_4/Cr_2O_3$ duplex oxide scale/metal substrate interface, a thin and non-continuous SiO_2 layer is present for all exposure times (Fig. 4 (d) and (f)). TiO_2 precipitates are also observable under the SiO_2 layer, due to their high thermodynamic stability, as discussed in the previous paragraph.~~

In addition, the mass increase observed after 3000 hours can equally be related to the presence of a thin and non-continuous SiO_2 layer at the interface between Cr_2O_3 and the metallic substrate (Fig. 4 (f)) and of TiO_2 precipitates at the outer part of steel.

After ageing in oxidising atmospheres, LNF coatings evolve in a similar way, leading to the formation of NiO and to a new LNF perovskite with a higher Fe content [17], in agreement with the fact that the $LaNi_{1-x}Fe_xO_3$ structure becomes more stable with increasing x [60]. NiO formation occurs together with Ni depletion toward the metal interface [17]. In parallel, Montero et al. [26] observe the presence inside the coating of Ni-Cr oxides that might appear from the reaction of NiO with the Cr released from the stainless steel. Basu et al. [17] relate the release of NiO with a partial substitution of perovskite by Cr. Moran Ruiz et al. [61] equally observe Cr incorporation into the LNF structure. However, any of these studies does not report the formation of La_2O_3 phase.

3.3 $MnCo_2O_4$ coated K41X samples

Figure 6 (a) and (b) present the Co-Mn coating with 2:1 ratio deposited by PVD technique on K41X as-rolled sample after annealing in air at 800°C for 10 hours. EDX coupled with XRD analyses revealed that a single cubic $MnCo_2O_4$ spinel phase formed. This result is in agreement with Mn-Co-O phase diagram in air calculated with FactSage thermodynamics software by Bateni et al. [37] and with the study of Xia et al. [62] concerning the crystalline structure of $Mn_xCr_{3-x}O_4$ spinels. As shown in Fig. 6 (b), the Co-Mn coating presents a thickness of about 4 µm and good adherence with the metallic substrate. The coating layer is affected by a significant porosity in the inner part and a large number of vertical cracks at the outer part, that might have formed because of the thermal expansion coefficient difference with the substrate ($9.7 \cdot 10^{-6}$ K^{-1} for $MnCo_2O_4$ [7] versus $12.2 \cdot 10^{-6}$ K^{-1} for the substrate, at 800°C [17]). Below the coating, a Cr_2O_3 layer formed, with a thickness of about 1 µm, probably because of the easy oxygen inward diffusion through the high number of surface cracks and porosities present in Co-Mn spinel layer.

When ageing the $MnCo_2O_4$ coated K41X samples in Ar – 1 % H_2 – 9 % H_2O atmosphere, a negative weight change was observed during the first 1000 hours (Fig. 1). The weight decrease was the highest after 200 hours of exposure, when $MnCo_2O_4$ decomposition took place, leading to the appearance of Co metallic nodules of about 3µm diameter in top of a MnO continuous thin layer, as revealed by EDX (Fig. 6 (c) and (d)) and XRD analyses. Below the MnO scale, a $(Cr,Mn)_3O_4$ layer equally formed . After 1000 hours, the nodules are connected by a (Mn,Fe)O phase, as illustrated by SEM elementary mapping (Fig. 7). This microstructure is found after 3000 hours of exposure (Fig. 6 (e) and (f)), with an increased amount of (Mn,Fe)O phase. Indeed, Mn and Fe present a good diffusivity through chromia scales [57]. Moreover, it was shown that in reducing atmospheres Mn diffuses outward most favourably than in oxidising atmospheres, in order to form oxides with or without other

elements [44]. As a consequence, the positive mass variation observed after 3000 hours ageing can be related to a higher quantity of (Mn,Fe)O together with the thickening of $(Cr,Mn)_3O_4/Cr_2O_3$ duplex scale.

The mass increase can also be related to Si and Ti oxides formation (Fig. 6 (d) and (f)). As shown in Fig. 7 (d), after 1000 hours of thermal treatment, a thin and continuous SiO_2 layer formed at the interface with the metallic substrate, but it was equally observed after 200 hours ageing. Silica was present only as isolated particles for the uncoated sample exposed for 200 hours [3]. It can be supposed that the annealing treatment of Co-Mn metallic deposit, done for 10 hours at 800°C in air, initiated the growth of silica particles that joined during the 200 hours ageing in H_2-H_2O. A synergetic effect seems to occur, as normally more than 1000 hours are necessary to as-rolled K41X to form continuous silica in H_2-H_2O atmosphere [3].

The decomposition of Co-Mn spinel coatings during ageing in oxidising atmospheres was never reported in the literature. At most, Co/Mn ratio decreased, probably because of the Mn outward diffusion from the metallic substrate or the high volatility of Co atom, as observed by Choi et al. [33] after exposure of $MnCo_2O_4$ coatings in air at 800°C. Some Fe enrichment of the spinel coating is equally observed by many authors [32,63,64], in agreement with the fact that $(Mn,Fe)_3O_4$ and $(Mn,Fe,Co)_3O_4$ formation was reported to be thermodynamically favourable in oxidising conditions [65]. Nevertheless, Co-Mn spinel coatings are efficient in avoiding outward Cr migration [64,66,67].

Under H_2/H_2O, the decomposition of Co-Mn spinel in metallic Co and Mn oxides observed in the present study is in agreement with the observations done by different authors during coating densification involving a step in different reducing atmospheres at 800°C [63,66]. It was equally observed by Mardare et al. [38] after ageing different $(Mn,Co)_3O_4$ spinel coatings in 97 % H_2 – 3 % H_2O, leading to the formation of metallic Co and MnO. All these findings imply that Co oxides are not stable at low oxygen partial pressures, as supported by the

Ellingham-Richardson diagram [49]. Indeed, the oxygen partial pressure corresponding to Ar - 1 % H_2 - 9 % H_2O atmosphere is of 10^{-16} bar. This value is lower than the oxygen partial pressure for CoO formation, of 10^{-15} bar, but much higher than the value of 10^{-30} bar needed for MnO formation. Even if the formation of iron oxides is also possible above 10^{-18} bar, they were not observed in the present case; however, some Fe doping of MnO oxide was revealed after 1000 hours ageing by SEM elementary mapping (Fig. 7).

Besides Co-Mn spinel decomposition, the negative mass change observed for $MnCo_2O_4$ coated K41X samples until 1000 hours of exposure, might equally be caused by a loss of Co at the sample surface due to formation of volatile Co species, following the reaction [68]:

$$Co_3O_{4(s)} + 3\ H_2O_{(g)} = 3\ Co(OH)_{2(g)} + ½\ O_{2(g)} \quad (1)$$

This mechanism is reported by Stanislowski et al. [41] at 800°C under humidified air and supposed by Mardare et al [38] in order to explain to total absence of metallic Co in the latter case after 500 hours of exposure at 800°C in 97 % H_2 – 3 % H_2O.

Co volatilization might have occurred in Ar – 1 % H_2 – 9 % H_2O, as the atomic percent of Co present at the sample surface after 3000 hours has decreased compared to $MnCo_2O_4$ stoichiometry (around 18 at. % instead of 28.5 at. % initially). However, the Co content might have apparently decreased because of Mn and, in a much lesser extent, of Fe outward diffusion. Indeed, a decrease of Co/Mn ratio was measured by EDX analyses, from 2:1 in the initial coating to 1:2 after 200 hours of exposure and 1:3 after 3000 hours of exposure. At the same time, any Co enrichment was not observed at the inner parts of the scale (contrarily to what it was noticed by Mardare et al. [38]). Nevertheless, even if the water vapour content is more important in our study, the supposed evaporation is less significant than in 97 % H_2 – 3 % H_2O, as even after 3000 hours at 800°C in Ar - 1 % H_2 - 9 % H_2O, Co nodules are still present (Fig. 6 (f)).

Another possible reason for the mass loss, much less reported in the literature, might be related to Mn evaporation that occurs in H_2-H_2O atmospheres, as shown by Stanilowski et al. [41] and attributed to the formation of $MnH_{2(g)}$. In these conditions, Mn evaporation is about 1 order of magnitude higher than Cr vaporisation rate. The authors observed that Mn evaporation from $(Cr,Mn)_3O_4$ spinel occurs with MnO grains formation. Indeed, the latter phase is present in our case for the time dwells where the negative mass variation was observed, supporting the Mn evaporation hypothesis, but without firmly confirming it.

As shown by SEM cross-section analyses after 3000 hours ageing (Fig. 6 (f)), all Cr-containing oxides are localised in the inner part of the oxide scale and not in contact with the atmosphere; as expected, Cr evaporation does not take place in H_2-H_2O atmosphere in presence of Co-Mn coating.

3.4 Co_3O_4 coated K41X samples

The surface and cross-section of PVD-deposited Co_3O_4 coating after crystallisation in air at 800°C for 10 hours are shown in Fig. 8 (a) and (b). EDX coupled with XRD analyses revealed the formation of single cubic Co_3O_4 spinel phase. The coating presents a significant number of porosities and vertical cracks up to the external surface. As previously supposed for Co-Mn spinel coating, these cracks might have formed because of thermal expansion coefficient difference with the substrate (9.3 10^{-6} K^{-1} for Co_3O_4 versus 12.2 10^{-6} K^{-1} for the substrate, at 800°C [7,17]).

The thickness of Co_3O_4 coating is about 7.5 µm. Below the coating, a Cr_2O_3 layer with a thickness of about 2-3 µm formed, but is much larger that for $MnCo_2O_4$ coated sample, as already reported in the literature after air exposure of the two compositions [69].

Co_3O_4 coated K41X samples present significant negative mass changes for all exposures periods up to 3000 hours in Ar - 1%H_2 - 9%H_2O (Fig. 1). On the basis of EDX and XRD analyses, this behaviour was explained through the complete reduction of the oxide phase to metallic Co, taking place from the first exposure instants under H_2/H_2O atmosphere (Fig. 8 (c) and (d)). As a consequence of Co_3O_4 reduction, Co islands of about 5 - 30 µm lateral size, separated by empty spaces of a few µm large, can be observed for all periods up to 1000 hours, when any significant mass or microstructure change does not occur. Nevertheless, some Mn diffusion through Cr_2O_3 layer occurs, leading to the formation of a very thin layer (about 1 µm thick) of $(Mn,Cr)_3O_4$ at the interface between Co islands and Cr_2O_3. At 3000 hours, the Co islands have coalesced forming a continuous porous layer at the sample surface (Fig. 8 (e) and (f)). In parallel, MnO phase, revealed by SEM elementary mapping (Fig. 9) and XRD analyses, appeared in between Co islands. Two possible phenomena might have led to the formation of this phase: Mn fast diffusion through Cr_2O_3 layer and its reaction with oxidant species or the evaporation of Mn from $(Cr,Mn)_3O_4$ phase, that is associated with the appearance of MnO grains (as described by Stanilowski et al. in H_2 atmospheres [41]). The negative mass change becomes lower after 3000 hours of exposure, but probably related to the increase of $(Cr,Mn)_3O_4/Cr_2O_3$ duplex layer thickness. The negative mass change observed in the present study, might be caused by a loss of Co at the sample surface due to formation of volatile Co species, according to the Eq. 1, as reported by Stanislowski et al [41] at 800°C under humidified air and supposed by Mardare et al [38] at 800°C in 97 % H_2 – 3 % H_2O. However, if Co volatilisation occurs in our case, it should have a small contribution, as any change in the mass variation was not observed during the first 1000 hours of exposure and any significant variation of the coating thickness did not occur. Indeed, after 200 and 1000 hours the average thickness of the Co metallic layer, of 5 µm, corresponds to the initial PVD coating thickness, before crystallisation treatment. Mn evaporation might equally occur once

$(Cr,Mn)_3O_4$ spinel forms in top of Cr_2O_3 layer [41]; however, it should be very limited, as up to 1000 hours $(Cr,Mn)_3O_4$ layer is extremely thin.

This behaviour was not observed by Deng at al. after exposition of Co_3O_4 coating in air at 800°C [70]. Furthermore, Froitzheim et al. [71] and Wu et al. [69] showed that the spinel phase results from the exposition of metallic Co coatings in air at 800°C. However, the decomposition observed in H_2-H_2O atmosphere is in agreement with the observations done by Mardare et al. [38] showing that Co oxides are not stable at low oxygen partial pressures, as supported by the Ellingham-Richardson diagram [49]. The observed behaviour is equally in agreement with the study of Sachitanand et al. [72], where the exposure of PVD metallic Co coated Fe-22Cr ferritic steel in Ar-5%H_2-3%H_2O atmosphere leads to Co nodules and Co particles dispersed in top of and respectively inside $(Cr,Mn)_3O_4/Cr_2O_3$ layer. However, mass loss was not observed in this last case. There was no Cr presence after 3000 hours of exposure, showing that Co_3O_4 coating is efficient in preventing Cr evaporation phenomena in H_2-H_2O atmosphere, as already reported in oxidising atmospheres [69,70,72].

As shown in Fig. 9, after 3000 hours of exposure, a continuous SiO_2 layer can be observed at the interface with the metallic substrate, but it was already present after 200 hours ageing. As reported in literature by Shaigan el al. [73], for 5 µm Co coatings on AISI 430 substrate, spalling occurs between SiO_2 and Cr_2O_3 layer. Spalling was not observed in the present study up to 3000 hours of exposure. However, even if Co_3O_4 coating seems to be efficient in avoiding the growth of non-protective Fe-rich oxides and in preventing Cr evaporation phenomena, the presence of SiO_2 continuous layer from short ageing times could become detrimental for the long term system integrity.

4. Conclusions

In order to prevent the formation of non-protective Fe-rich oxides and to improve the oxidation behaviour of K41X stainless steel in H_2/H_2O atmosphere at 800°C, four coatings were chosen and tested: $La_{0.8}Sr_{0.2}MnO_3$ (LSM) and $LaNi_{0.6}Fe_{0.4}O_3$ (LNF) perovskites; $MnCo_2O_4$ and Co_3O_4 spinels. LSM and LNF were deposited by screen printing and $MnCo_2O_4$ and Co_3O_4 by PVD technique.

All the tested coatings allow avoiding Fe-rich oxides growth during high temperature oxidation up to 3000 hours. Instead, protective $(Cr,Mn)_3O_4/Cr_2O_3$ duplex oxide scale formed between the metallic substrate and the coating from the first exposure instants. 8 at.% Fe enrichment was detected inside LSM coating after 3000 hours of exposure and (Mn,Fe)O oxide was found for $MnCo_2O_4$ coated sample. Nevertheless, any detrimental Fe oxide were not detected after 3000 hours ageing, even if their formation is thermodynamically possible in Ar-1%H_2-9%H_2O at 800°C.

Cr was not detected inside LSM, $MnCo_2O_4$ and Co_3O_4 coatings up to 3000 hours of exposure, indicating that these compositions were efficient in preventing Cr evaporation. Some Cr (2 at. %) was detected all over the thickness of LNF coating after 3000 hours ageing, indicating that it is able to limit Cr outward diffusion, but not completely block it.

For all tested coating compositions, SiO_2 formed at the interface between the $(Cr,Mn)_3O_4/Cr_2O_3$ duplex scale and the metallic substrate from the first exposure instants. For Co_3O_4 coated K41X steel, the presence of continuous SiO_2 layer might be detrimental for the long term system integrity, as spalling can occur between SiO_2 and Cr_2O_3 layer. However, in the present study, any spalling was not observed up to 3000 hours of exposure.

In conclusion, the four coatings tested in this study represent promising solutions to improve the oxidation resistance of K41X stainless steel in H_2/H_2O atmosphere at 800°C, avoiding the growth of Fe-rich oxides at least during 3000 hours of exposure.

Acknowledgements

This work was partially supported by French Research National Agency (ANR) (ICARE project, n°ANR-08-PANH-009).

The authors would like to thank Aperam Isbergues for K41X supply, F. Perry (PVDCo) and R. Laucournet (CEA) for coatings elaboration.

Data Availability

The raw/processed data required to reproduce these findings cannot be shared at this time as the data also forms part of an ongoing study.

References

[1] J.W.Fergus, Metallic interconnects for solid oxide fuel cells, Mater. Sci. Eng. (2005) A397 271-283.

[2] W.J. Quaddakers, J. Piron-Abellan, V. Shemet, L. Singheiser, Metallic interconnectors for solid oxide fuel cells - a review, Mater. High Temp. (2003) 20(2) 115–127.

[3] M.R. Ardigo, V. Parry, I. Popa, S. Chevalier, W. Chandra-Ambhorn, P. Phakpeetinan, Y. Wouters, Optimisation of metallic interconnects for hydrogen production by high temperature water vapour electrolysis, Defect and Diffusion Forum 323-325 (2012) 239-244.

[4] M.R. Ardigo-Besnard, I. Popa, O. Heintz, R. Chassagnon, M. Vilasi, F. Herbst, P. Girardon, S. Chevalier, Effect of surface finishing on the oxidation behaviour of a ferritic stainless steel, Appl. Surf. Sci., 412 (2017) 196-206.

[5] D. Young, High temperature oxidation and corrosion of metals, first ed., Elsevier, Great Britain, 2008.

[6] H. Kurokawa, C. P. Jacobson, L.C. DeJonghe, S. J. Visco, Chromium vaporization of bare and of coated iron–chromium alloys at 1073 K, Solid State Ion. 178 (2007) 287-296.

[7] A. Petric, H. Ling, Electrical conductivity and thermal expansion of spinels at elevated temperatures, J Am Ceramic Soc 90 (5) (2007) 1515-20.

[8] N. Shaigan, W. Qu, D.G. Ivey, W. Chen, A review of recent progress in coatings, surface modifications and alloy developments for solid oxide fuel cell ferritic stainless steel interconnects, J. Power Sources 195 (2010) 1529-1542.

[9] S. Chevalier, G. Bonnet, P. Fielitz, G. Strehl, S.Weber, G. Borchardt, J.C. Colson, J.P. Larpin, Effects of a Reactive Element on isothermal and cyclic oxidation of chromia-forming alloys: SEM/EDX, TEM and SIMS investigations, Mat. High Temp. 17 (2) (2000) 247-256.

[10] S. Chevalier, G. Bonnet, J.P. Larpin, J.C. Colson, The combined effect of refractory coatings containing reactive elements on high temperature oxidation behavior of chromia-forming alloys, Corr. Sci. 45 (2003) 1661–1673.

[11] S. Chevalier, Traitements de surface et nouveaux matériaux : Quelles solutions pour lutter contre la dégradation des matériaux à haute température, Editions Universitaires de Dijon collection Sciences, Dijon, 2007.

[12] S. Fontana, R. Amendola, S. Chevalier, P. Piccardo, G. Caboche, M. Viviani, R. Molins, M. Sennour, Metallic interconnects for SOFC: Characterisation of corrosion resistance and conductivity evaluation at operating temperature of differently coated alloys, J. Power Sources 171 (2007) 652-662.

[13] S. Fontana, S. Chevalier, G. Caboche, Metallic interconnects for solid oxide fuel cell: Effect of water vapour on oxidation resistance of differently coated alloys, J. Power Sources 193 (2009) 136-145.

[14] J.G. Grolig, J. Froitzheim, J.E. Svensson, Coated stainless steel 441 as interconnect material for solid oxide fuel cells: Oxidation performance and chromium evaporation, J. Power Sources 248 (2014) 1007-1013.

[15] R. Sachitanand, M. Sattari, J.E. Svensson, J. Froitzheim, The Oxidation of Coated SOFC Interconnects in Fuel Side Environments, Fuel Cells 16 (2016) 32-38.

[16] S.P. Jiang, Development of lanthanum strontium manganite perovskite cathode materials of solid oxide fuel cells: a review, J. Mater. Sci. 43 (2008) 6799-6833.

[17] R. N. Basu, F. Tietz, O. Teller, E. Wessel, H. P. Buchkremer, D. Stöver, $LaNi_{0.6}Fe_{0.4}O_3$ as a cathode contact material for solid oxide fuel cells, J. Solid State Electrochem. 7 (2003) 416-420.

[18] Z.G. Yang, G.G. Xia, G.D. Maupin, J.W. Stevenson, Evaluation of perovskite overlay coatings on ferritic stainless steels for SOFC interconnect applications, J. Electrochem. Soc. 153 (2006) A1852–A1858.

[19] I. Belogolovsky, X.D. Zhou, H. Kurokawa, P.Y. Hou, S. Visco, H.U. Anderson, Effects of surface-deposited nanocrystalline chromite thin films on the performance of a ferritic interconnect alloy, J. Electrochem. Soc. 154 (2007) B976–B980.

[20] C. Lee, J. Bae, Oxidation-resistant thin film coating on ferritic stainless steel by sputtering for solid oxide fuel cells, Thin Solid Films 516 (2008) 6432–6437.

[21] N. Orlovskaya, A. Coratolo, C. Johnson, R. Gemmen, Structural characterization of lanthanum chromite perovskite coating deposited by magnetron sputtering on an iron-based chromium-containing alloy as a promising interconnect material for SOFCs, J. Am. Ceram. Soc. 87 (2004) 1981–1987.

[22] J.H. Zhu, Y. Zhang, A. Basu, Z.G. Lu, M. Paranthaman, D.F. Lee, E.A. Payzant, $LaCrO_3$-based coatings on ferritic stainless steel for solid oxide fuel cell interconnect applications, Surf. Coat. Technol. 177 (2004) 65–72.

[23] C.J. Fu, K.N. Sun, N.Q. Zhang, D.R. Zhou, Effects of protective coating prepared by atmospheric plasma spraying on planar SOFC interconnect, Rare Met. Mat. Eng. 35 (2006) 1117–1120.

[24] C.L. Chu, J.Y. Wang, S.Y. Lee, Effects of $La_{0.67}Sr_{0.33}MnO_3$ protective coating on SOFC interconnect by plasma-sputtering Int. J. Hydr. Energy 33 (2008) 2536–2546.

[25] Z.G. Yang, G.G. Xia, G.D. Maupin, J.W. Stevenson, Conductive protection layers on oxidation resistant alloys for SOFC interconnect applications Surf. Coat. Technol. 201 (2006) 4476–4483.

[26] X. Montero, F. Tietz, D. Stöver, M. Cassir, I. Villarreal, Comparative study of perovskites as cathode contact materials between an La(0.8)Sr(0.2)FeO(3) cathode and a Crofer22APU interconnect in solid oxide fuel cells, J. Power Sources 188 (2009) 148-155.

[27] J.H. Kim, R.H. Song, S.H. Hyun, Effect of slurry-coated LaSrMnO(3) on the electrical property of Fe-Cr alloy for metallic interconnect of SOFC, Solid State Ion. 174 (2004) 185–191.

[28] C.L Chu, J.Y. Wang, S. Lee, Effects of $La_{0.67}Sr_{0.33}MnO_3$ protective coating on SOFC interconnect by plasma-sputtering Int. J. Hydr. Energy, 33 (2008) 2536-2546

[29] C.L. Chu, J. Lee, T.H. Lee, Y.N. Cheng, Oxidation behavior of metallic interconnect coated with La–Sr–Mn film by screen painting and plasma sputtering, Int. J. Hydr. Energy 34 (2009) 422-434.

[30] M. R. Ardigo, I. Popa, S. Chevalier, V. Parry, A. Galerie, P. Girardon, F. Perry, R. Laucournet, A. Brevet, Effect of coatings on a commercial stainless steel for SOEC interconnect application in anode atmosphere. Proceeding of the 13th International Symposium on Solid Oxide Fuel Cells October 6-11, 2013, Okinawa, Japan.

[31] X. Chen, P. Y. Hou, C. P. Jacobson, S. J. Visco, L. C. De Jonghe, Protective coating on stainless steel interconnect for SOFCs: oxidation kinetics and electrical properties, Solid State Ion. 176 (2005) 425–433.

[32] B. Hua, J. Pu, W. Gong, J. Zhang, F. Lu, L. Jian, Cyclic oxidation of Mn–Co spinel coated SUS 430 alloy in the cathodic atmosphere of solid oxide fuel cells, J. Power Sources 185 (2008) 419–422.

[33] J.J. Choi, J. Ryu, B.D. Hahn, W.H. Yoon, B.K. Lee, D.S. Park, Dense spinel $MnCo_2O_4$ film coating by aerosol deposition on ferritic steel alloy for protection of chromic evaporation and low-conductivity scale formation, J. Mater. Sci. 44 (2009) 843-848.

[34] P.E. Gannon, V.I. Gorokhovsky, M.C. Deibert, R.J. Smith, A. Kayani, P.T. White, S. Sofie, Z. Yang, D. McCready, S. Visco, C. Jacobson, H. Kurokawa, Enabling inexpensive metallic alloys as SOFC interconnects: An investigation into hybrid coating technologies to deposit nanocomposite functional coatings on ferritic stainless steels, Inter. J. Hydr. Energy 32 (2007) 3672–3681.

[35] J. Wu, C. D. Johnson, Y. Jiang, R. S. Gemmen, X. Liu, Pulse plating of Mn-Co alloys for SOFC interconnect applications, Electrochem. Acta 54 (2008) 793–800.

[36] X. Montero, F. Tietz, D. Sebold, H.P. Buchkremer, A. Ringuede, M. Cassir, A. Laresgoiti, I. Villarreal, $MnCo_{1.9}Fe_{0.1}O_4$ spinel protection layer on commercial ferritic steels for interconnect applications in solid oxide fuel cells, J. Power Sources 184 (2008) 172-179.

[37] M. R. Bateni, P. Wei, X. Deng, A. Petric, Spinel coatings for UNS 430 stainless steel interconnects, Surf. & Coat. Techn 201 (2007) 4677–4684.

[38] C.C. Mardare, H. Asteman, M. Spiegel, A. Savan, A. Ludwig, Investigation of thermally oxidised Mn–Co thin films for application in SOFC metallic interconnects, Appl. Surf. Sci. 255 (2008) 1850-1859.

[39] C. Key, J. Eziashi, J. Froitzheim, R. Amendola, R. Smith, P. Gannon, Methods to Quantify Reactive Chromium Vaporization from Solid Oxide Fuel Cell Interconnects, J. Electrochem. Soc. 161 (2014) C373-C381.

[40] E. J. Opila, D. L. Myers, N. S. Jacobson, I. M. B. Nielsen, D. F. Johnson, J. K. Olminsky, M. D. Allendorf, Theoretical and experimental investigation of the thermochemistry of $CrO_2(OH)_{(2)(g)}$ J. Phys. Chem. A 111 (2007) 1971-1980.

[41] M. Stanislowski, E. Wessel, K. Hilpert, L. Singheiser, Chromium vaporization from high temperature alloys I. Chromia-forming steels and the influence of outer oxide layers, J. Electrochem. Soc. 154 (4) (2007) A295-A306.

[42] S. Chevalier, J. Favergeon, French Activity on High Temperature Corrosion in Water Vapor, Trans Tech Publications Ltd, Durntern-Zurich, 2014, p. 131.

[43] J.Q. LI, P. Xiao, Fabrication and characterisation of $La_{0.8}Sr_{0.2}MnO_3$/metal interfaces for application in SOFCs, J. European Ceram. Soc. 21 (2001) 659-668.

[44] Y. Liu, Performance evaluation of several commercial alloys in a reducing environment, J. Power Sources 179 (2008) 286-291.

[45] Z. Yang, G.G. Xia, P. Singh, J.W. Stevenson, Electrical contacts between cathodes and metallic interconnects in solid oxide fuel cells, J. Power Sources 155 (2006) 246-252.

[46] W.J. Quadakkers, H. Greiner, M. Hansel, A. Pattanaik, A.S. Khanna, W. Mallener, Compatibility of perovskite contact layers between cathode and metallic interconnector plates of SOFCs, Solid State Ion. 91 (1996) 55-67.

[47] S.P.S. Badwal, R. Deller, K. Foger, Y. Ramprakash, J.P. Zhang, Interaction between chromia forming alloy interconnects and air electrode of solid oxide fuel cells, Solid State Ion. 99 (1997) 297-310.

[48] Y.D. Zhen, S.P. Jiang, S. Zhang, V. Tan, Interaction between metallic interconnect and constituent oxides of (La,Sr)MnO_3 coating of solid oxide fuel cells, J. European Ceram . Soc. 26 (2006) 3253-3264.

[49] M. Hasegawa, Chapter 3.3 - Ellingham Diagram, in: S. Seetharaman, A. McLean, R. Guthrie, S. Sridhar, Treatise on Process Metallurgy Volume 1: Process Fundamentals, Elsevier Ldt., Oxford, 2014, pp. 507-516.

[50] N. Caillol, M. Pijolat, E. Siebert, Investigation of chemisorbed oxygen, surface segregation and effect of post-treatments on $La_{0.8}Sr_{0.2}MnO_3$ powder and screen-printed layers for solid oxide fuel cell cathodes, Appl. Surf. Sci. 253 (2007) 4641-4648.

[51] Q.H. Wu, M. Liu, W. Jaegermann, X-ray photoelectron spectroscopy of $La_{0.5}Sr_{0.5}MnO_3$, Mat. Lett. 59 (2005) 1480-1483.

[52] H. Hwang, G.M. Choi, The effects of LSM coating on 444 stainless steel as SOFC interconnect, J. Electroceram. 22 (2009) 67-72.

[53] T. Jin, K. Lu, Chemical compatibility between Sr-doped lanthanum manganite air electrode and AISI 441 interconnect, Int. J. Hydr. Energy 36 (2011) 4440-4448.

[54] S.P. Simner, M.D. Anderson, G.G. Xia, Z. Yang, L.R. Pederson, J.W. Stevenson, SOFC Performance with Fe-Cr-Mn Alloy Interconnect, J. Electrochem. Soc. 152 (2005) A740-A745.

[55] P. Yang, C.K. Liu, J.Y. Wu, W.J. Shong, R.Y. Lee, C.C. Sung, Effects of pre-oxidation on the microstructural and electrical properties of $La_{0.67}Sr_{0.33}MnO_{3-\delta}$ coated ferritic stainless steels, J. Power Sources 213 (2012) 63-68.

[56] C.L. Chu, J.Y. Wang, S.Y. Lee, Effects of $La_{0.67}Sr_{0.33}MnO_3$ protective coating on SOFC interconnect by plasma-sputtering, Int. J. Hydrogen Energy 33 (2008) 2536–2546.

[57] M.G.C. Cox, B. McEnaney, V.D. Scott, A chemical diffusion model for partitioning of transition elements in oxide scales on alloys, Philos. Mag. 26 (1972) 839-851.

[58] R. Lacey, A. Pramanick, J.C. Lee, J.I. Jung, B. Jiang, D.D. Edwards, R. Naum, S.T. Misture, Evaluation of Co and perovskite Cr-blocking thin films on SOFC interconnects, Sol. St. Ion. 181 (2010) 1294-1302.

[59] T. Komatsu, H. Arai, R. Chiba, K. Nozawa, M. Arakawa, K. Sato, Cr Poisoning suppression in solid oxide fuel cells using LaNi(Fe)O_3 electrodes, Electrochem. Solid Sate Let. 9 (2006) A9-A12.

[60] R. Chiba, F. Yoshimura, Y. Sakurai, An investigation of $LaNi_{1-x}Fe_xO_3$ as cathode material for solid oxide fuel cells, Solid State Ionics 124 (1999) 281-288.

[61] A. Moran-Ruiz, K. Vidal, M.A. Laguna-Bercero, A. Larranaga, M.I. Arriortua, $LaNi_{0.6}Co_{0.4}O_{3-\delta}$ dip-coated on Fe-Cr mesh as a composite cathode contact material on intermediate solid oxide fuel cells, J. Power Sources 248 (2014) 1067-1076.

[62] G. Xia, Z. Yang, J. Stevenson, Manganese-cobalt spinel oxides as surface modifiers for stainless steel interconnects of solid oxide fuel cells, ECS Trans. 1 (2006) 325-332.

[63] W. Wei, W. Chen, D. G. Ivey, Oxidation resistance and electrical properties of anodically electrodeposited Mn–Co oxide coatings for solid oxide fuel cell interconnect applications, J. Power Sources 186 (2009) 428-434.

[64] Z. Yang, G.G. Xia, C.M. Wang, Z. Nie, J. Templeton, J.W. Stevenson, P. Singh, Investigation of iron–chromium–niobium–titanium ferritic stainless steel for solid oxide fuel cell interconnect applications, J. Power Sources 183 (2008) 660-667.

[65] C. Gleitzer, Diversity and complexity of the wustite solid solutions I-tentative rationalization of the miscibility data and classification of the wustite ternary fields and of the postsaturation reactions, Mater. Res. Bull. 15 (1980) 507.

[66] Z. Yang, G.-G. Xia, X.-H. Li, J. W. Stevenson, $(Mn,Co)_3O_4$ spinel coatings on ferritic stainless steels for SOFC interconnect applications, Int. J. Hydrogen Energy 32 (2007) 3648-3654.

[67] X. Xin, S. Wang, J. Qian, C. Lin, Z. Zhan, T. Wen, Development of the spinel powder reduction technique for solid oxide fuel cell interconnect coating, Int. J. Hydrogen Energy 37 (2012) 471-476.

[68] C. Gindorf, L. Singheiser, K. Hilpert, in: International Union of Pure and Applied Chemistry (IUPAC) Conferences on High Temperature Materials Chemistry (HTMC-XI), University of Tokyo, 2003, p. 384.

[69] J. Wu, C.D. Johnson, R.S. Gemmen, X. Liu, The performance of solid oxide fuel cells with Mn–Co electroplated interconnects cathode current collector, J. Power Sources 189 (2009) 1106-1113.

[70] X. Deng, P. Wei, M.Reza Bateni, A. Petric, Cobalt plating of high temperature stainless steel interconnects, J. Power Sources 160 (2006) 1225 – 1229.

[71] J. Froitzheim, S. Canovic, M. Nikumaa, R. Sachitanand, L.G. Johansson, J.E. Svensson, Long term study of Cr evaporation and high temperature corrosion behaviour of Co coated ferritic steel for solid oxide fuel cell interconnects, J. Power Sources 220 (2012) 217-227.

[72] R. Sachitanand, M. Sattari, J.E. Svensson, J. Froitzheim, The oxidation of coated SOFC interconnects in fuel side environments, Fuel Cells 16 (2016) 32-38.

[73] N. Shaigan, D.G. Ivey, W. Chen, Co/$LaCrO_3$ composite coatings for AISI 430 stainless steel solid oxide fuel cell interconnects, J. Power Sources 185 (2008) 331-337.

Figure captions

Figure 1: Surface weight change of uncoated and coated K41X samples after 200, 1000 and 3000 hours ageing at 800°C in Ar – 1 % H_2 – 9 % H_2O atmosphere.

Figure 2: Surface and cross-section microstructures of LSM coated K41X samples (a-b) before ageing, (c-d) after 200 hours and (e-f) after 3000 hours ageing at 800°C in Ar – 1 % H_2 – 9 % H_2O atmosphere.

Figure 3: SEM-EDX elementary mapping of LSM coated K41X samples after 3000 hours ageing at 800°C in Ar – 1 % H_2 – 9 % H_2O atmosphere.

Figure 4: Surface and cross-section microstructures of LNF coated K41X samples (a-b) before ageing, (c-d) after 200 hours and (e-f) after 3000 hours ageing at 800°C in Ar – 1 % H_2 – 9 % H_2O atmosphere.

Figure 5: SEM-EDX elementary mapping of LNF coated K41X samples after 200 hours ageing at 800°C in Ar – 1 % H_2 – 9 % H_2O atmosphere.

Figure 6: Surface and cross-section microstructures of $MnCo_2O_4$ coated K41X samples (a-b) before ageing, (c-d) after 200 hours and (e-f) after 3000 hours ageing at 800°C in Ar – 1 % H_2 – 9 % H_2O atmosphere.

Figure 7: SEM-EDX elementary mapping of $MnCo_2O_4$ coated K41X samples after 1000 hours ageing at 800°C in Ar – 1 % H_2 – 9 % H_2O atmosphere.

Figure 8: Surface and cross-section microstructures of Co_3O_4 coated K41X samples (a-b) before ageing, (c-d) after 200 hours and (e-f) after 3000 hours ageing at 800°C in Ar – 1 % H_2 – 9 % H_2O atmosphere.

Figure 9: SEM-EDX elementary mapping of Co_3O_4 coated K41X samples after 3000 hours ageing at 800°C in Ar – 1 % H_2 – 9 % H_2O atmosphere.

Figure 1

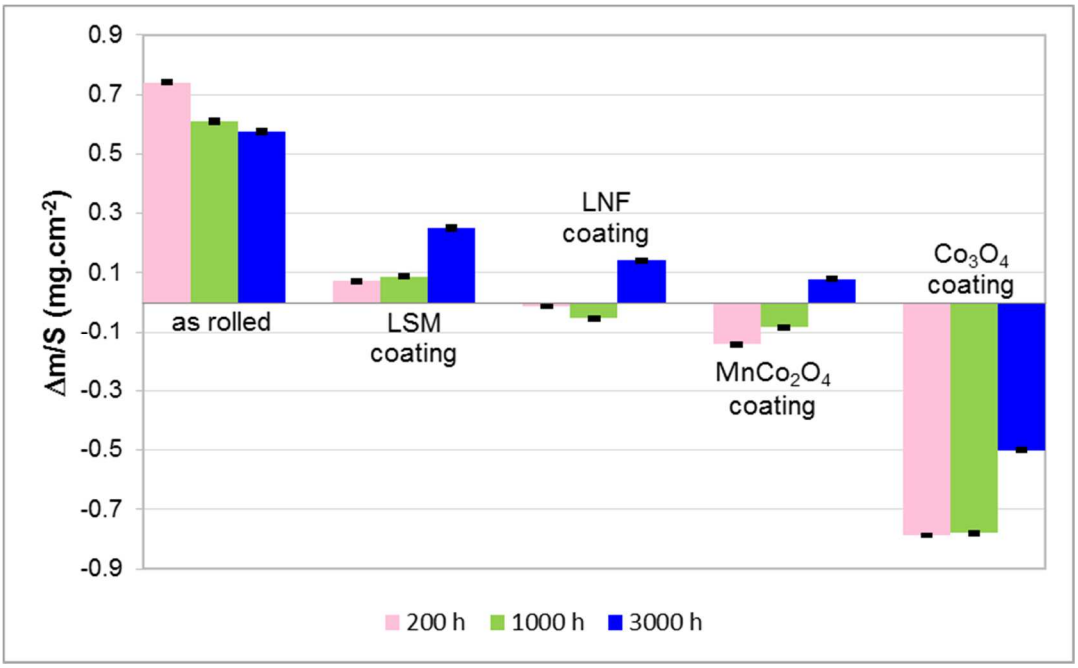
0.9
0.7
0.5
0.3
0.1
-0.1
-0.3
-0.5
-0.7
-0.9
Δm/S (mg.cm-2)
as rolled
LSM coating
LNF coating
MnCo2O4 coating
Co3O4 coating
200 h
1000 h
3000 h

Figure 2

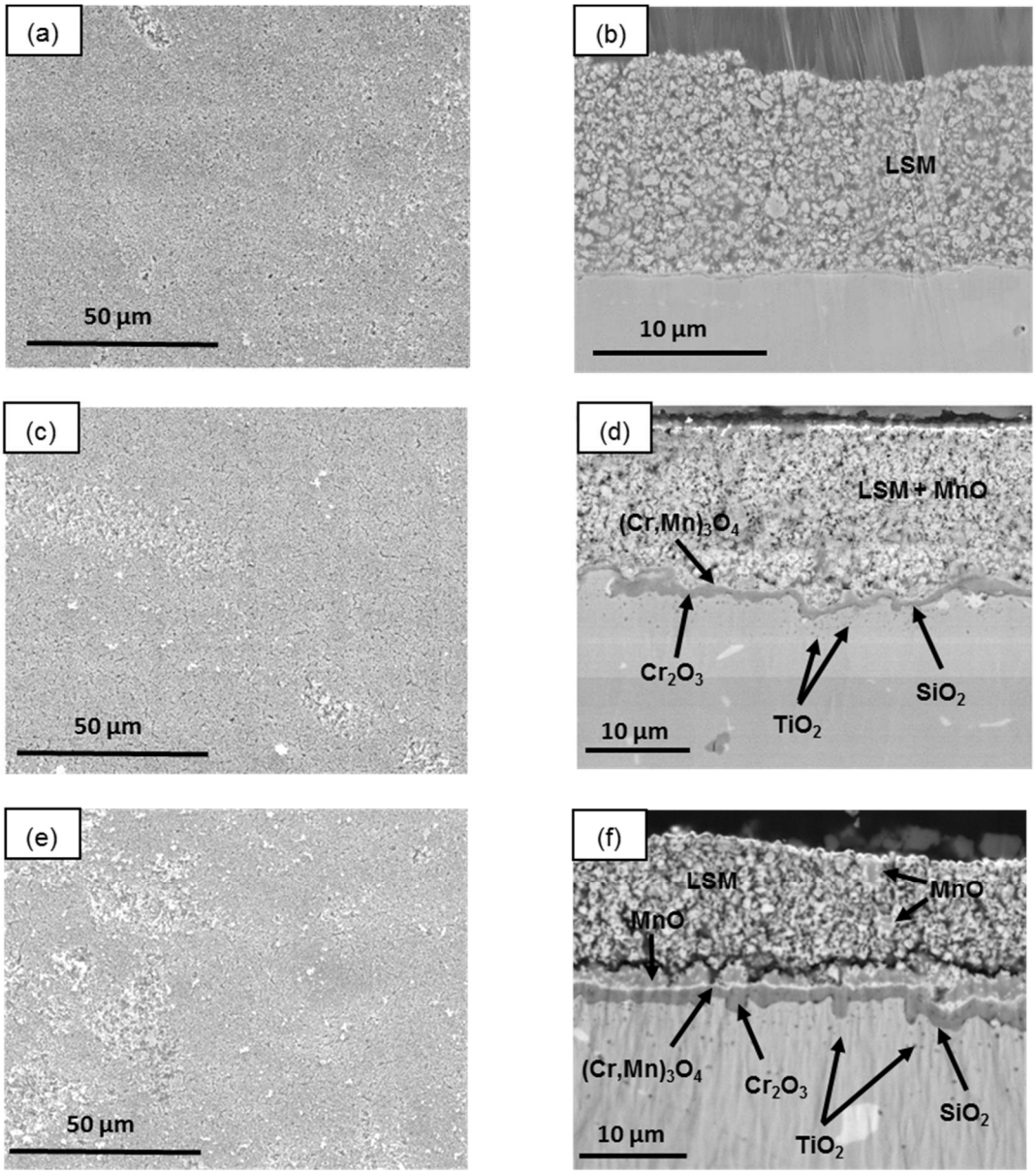
(a)
50 µm
(b)
LSM
10 µm
(c)
50 µm
(d)
LSM + MnO
(Cr,Mn)3O4
Cr2O3
TiO2
SiO2
10 µm
(e)
50 µm
(f)
LSM
MnO
MnO
(Cr,Mn)3O4
Cr2O3
TiO2
SiO2
10 µm

Figure 3

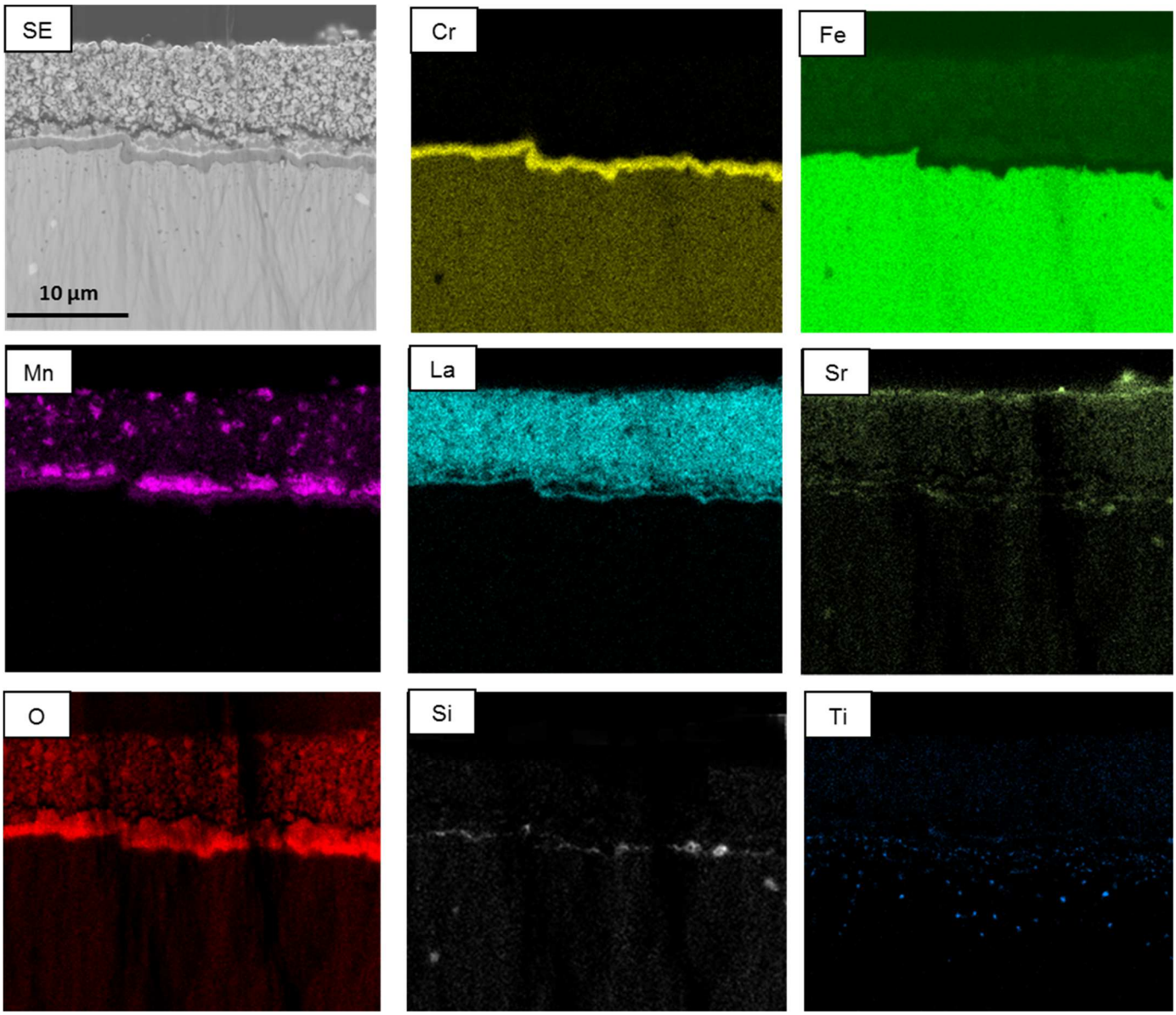

Figure 4

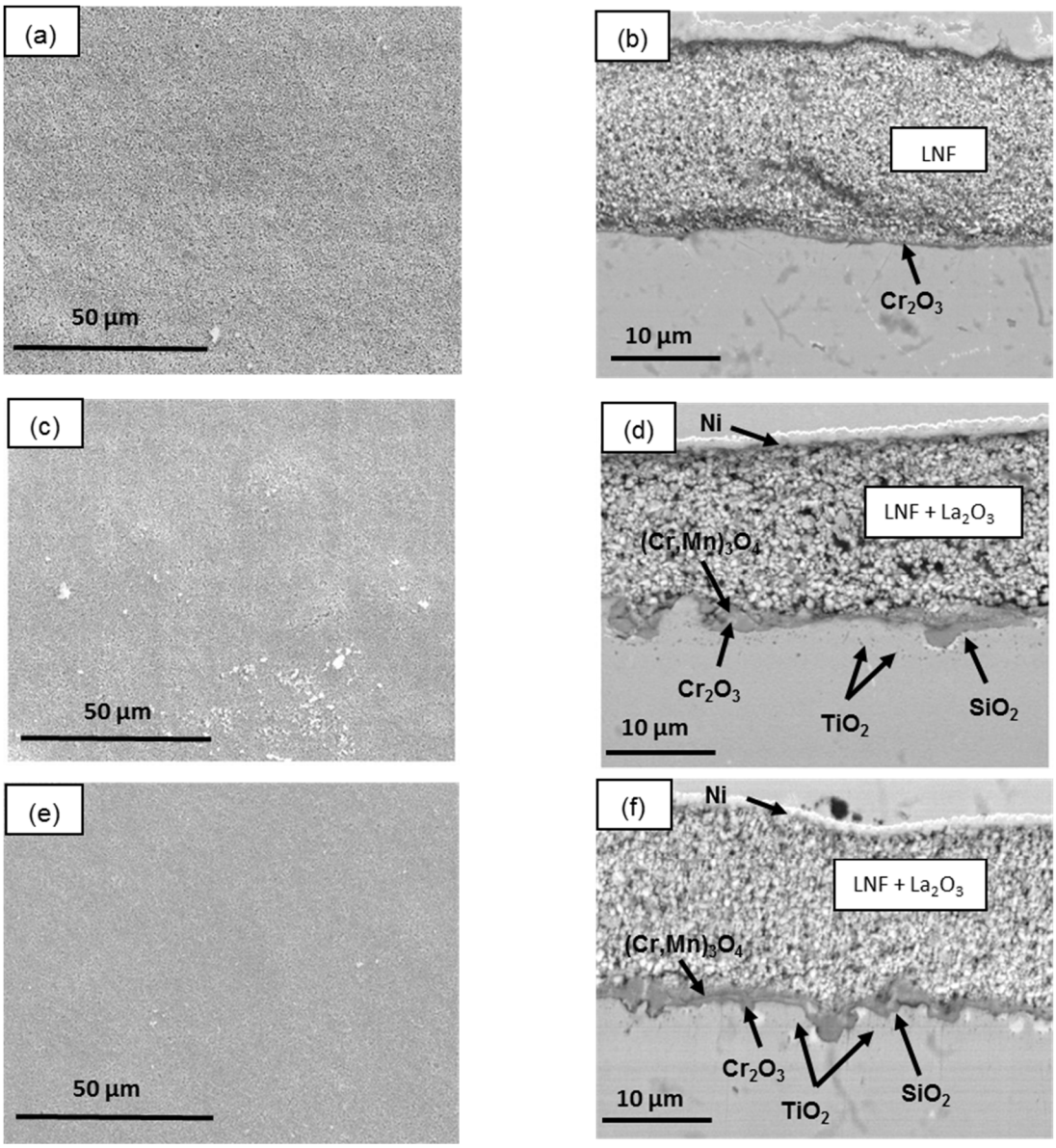
(a)
50 µm
(b)
LNF
Cr_2O_3
10 µm
(c)
50 µm
(d)
Ni
LNF + La_2O_3
$(Cr,Mn)_3O_4$
Cr_2O_3
TiO_2
SiO_2
10 µm
(e)
50 µm
(f)
Ni
LNF + La_2O_3
$(Cr,Mn)_3O_4$
Cr_2O_3
TiO_2
SiO_2
10 µm

Figure 5

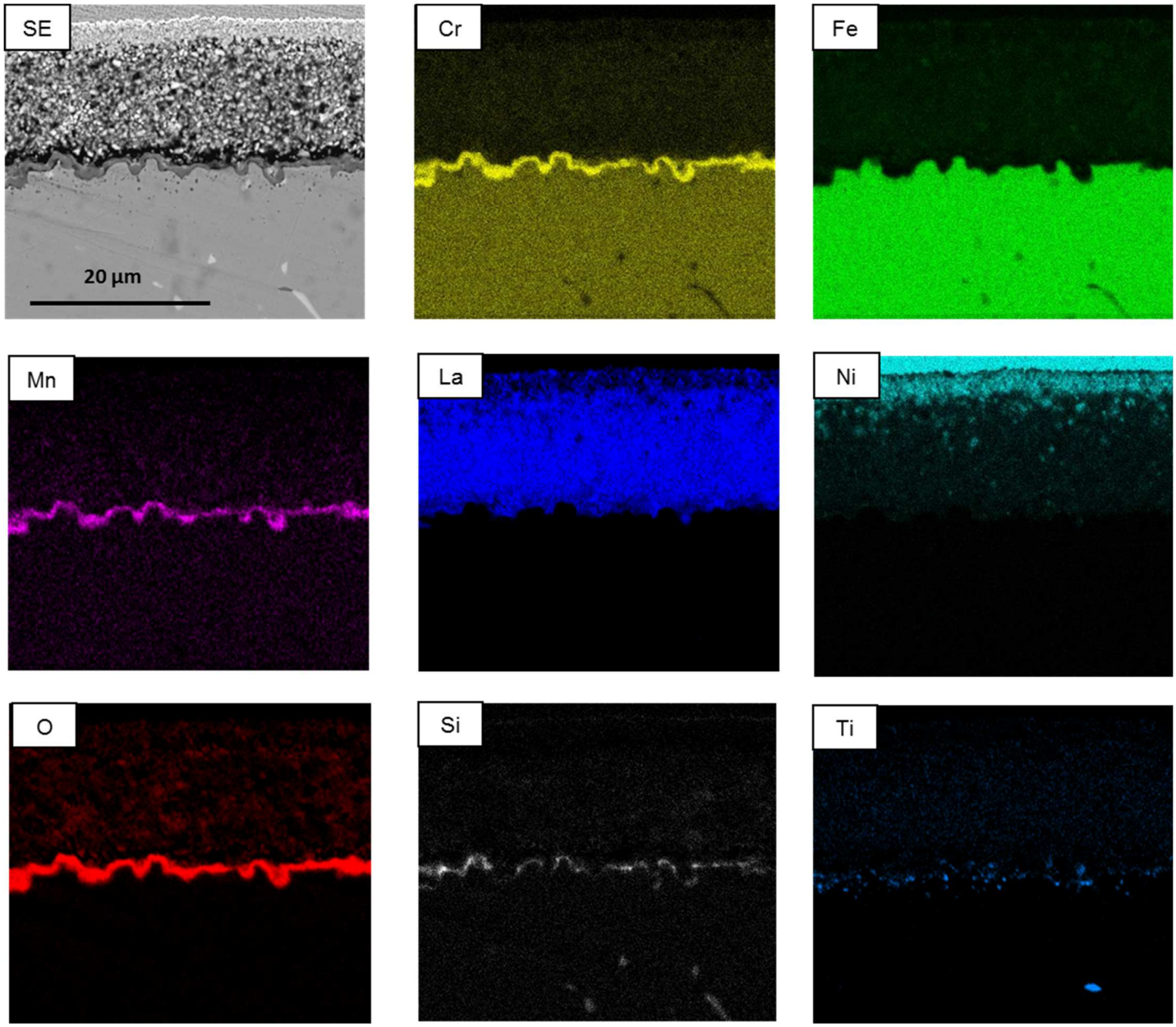

Figure 6

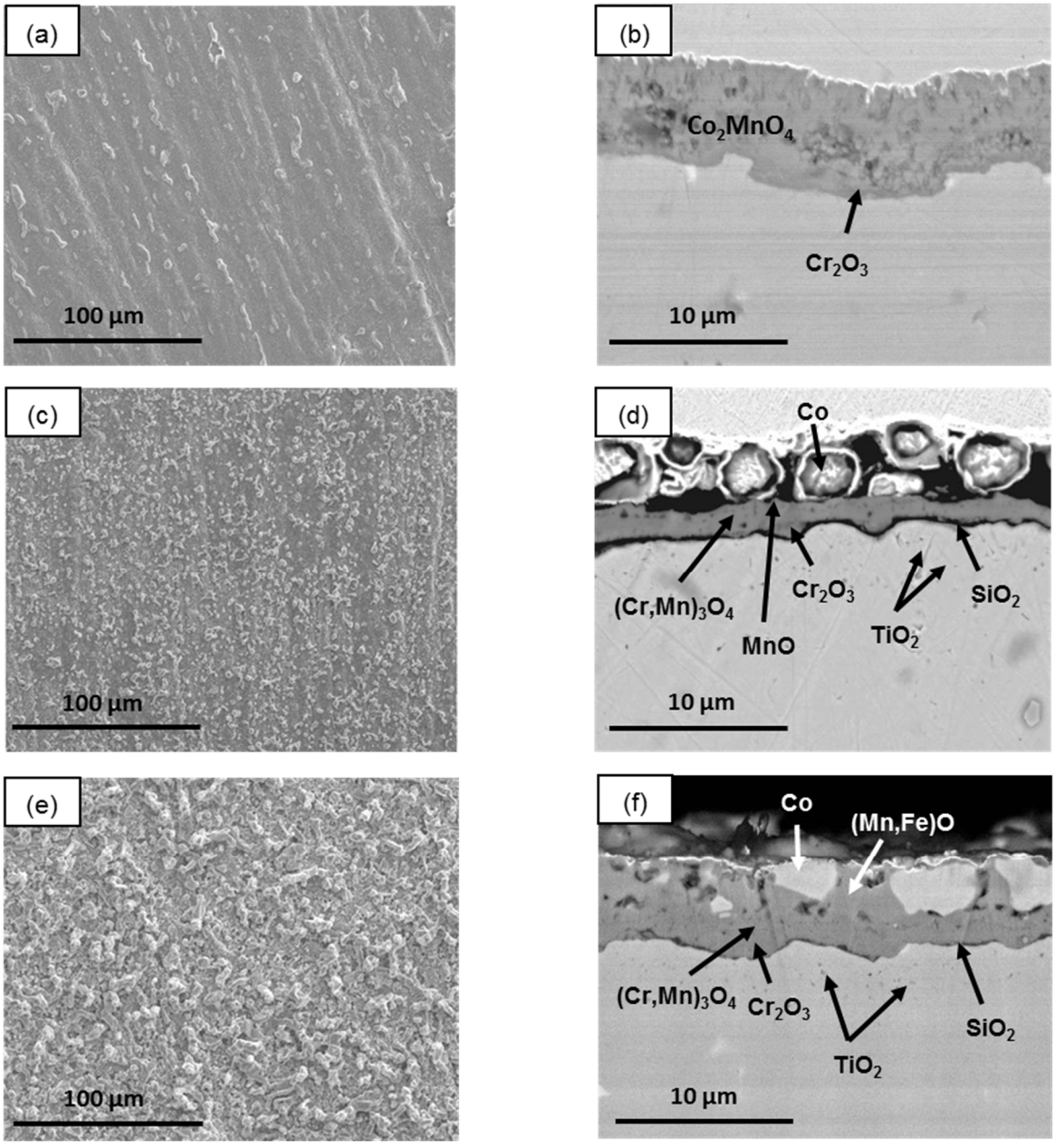
(a)
100 µm
(b)
Co_2MnO_4
Cr_2O_3
10 µm
(c)
100 µm
(d)
Co
$(Cr,Mn)_3O_4$
MnO
Cr_2O_3
TiO_2
SiO_2
10 µm
(e)
100 µm
(f)
Co
(Mn,Fe)O
$(Cr,Mn)_3O_4$
Cr_2O_3
TiO_2
SiO_2
10 µm

Figure 7

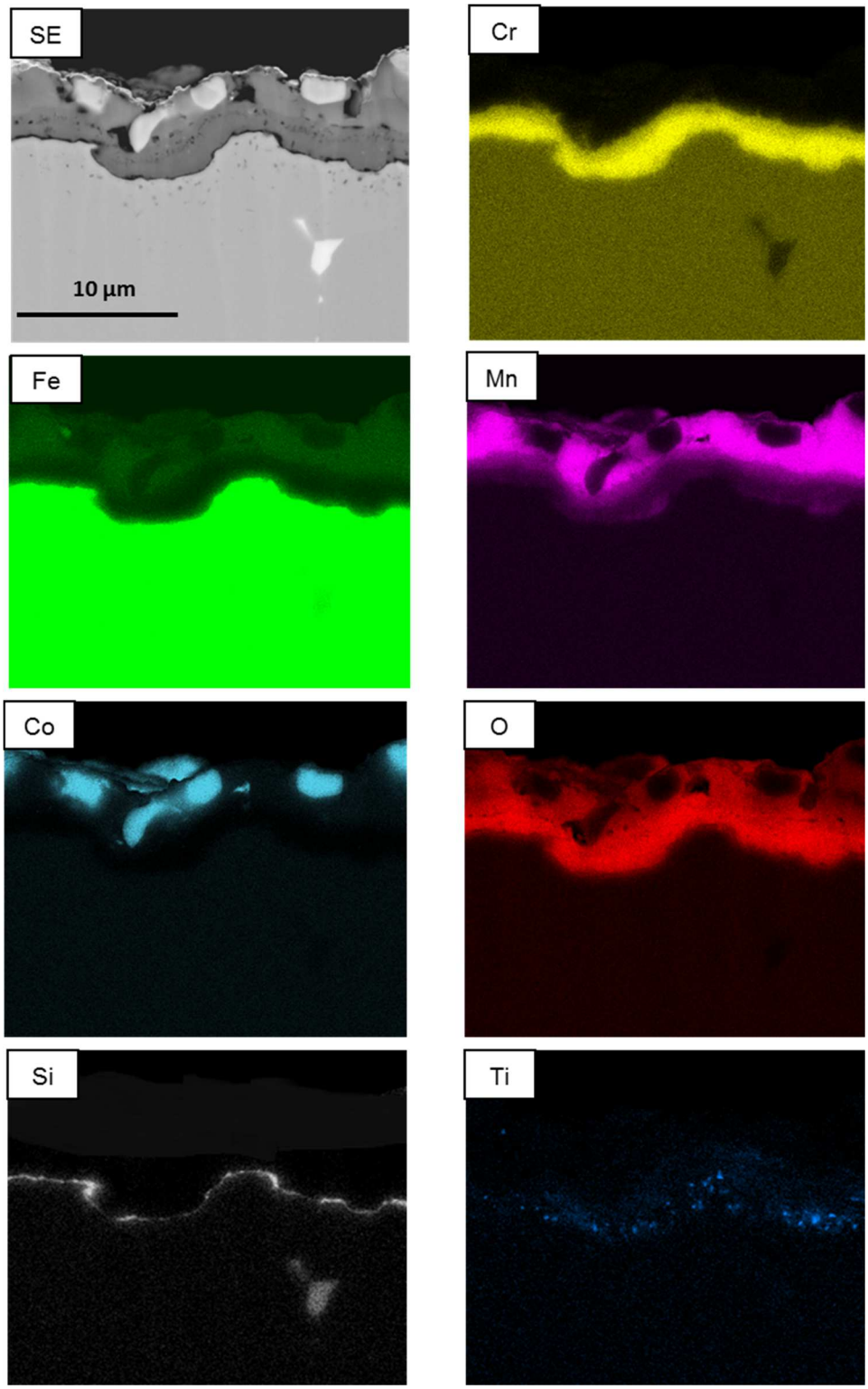

Figure 8

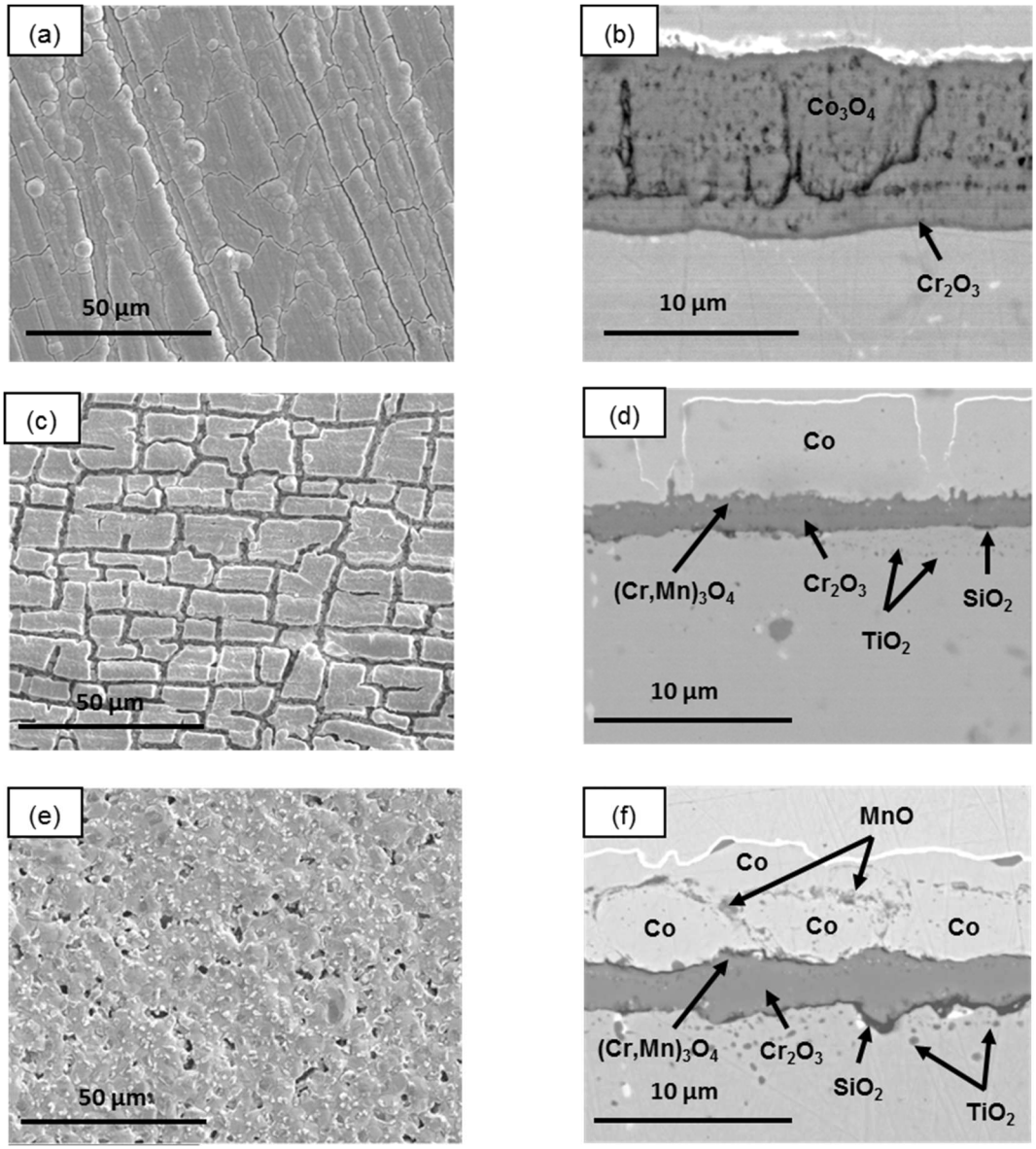
(a)
50 µm
(b)
Co_3O_4
Cr_2O_3
10 µm
(c)
50 µm
(d)
Co
$(Cr,Mn)_3O_4$
Cr_2O_3
TiO_2
SiO_2
10 µm
(e)
50 µm
(f)
MnO
Co
Co
Co
Co
$(Cr,Mn)_3O_4$
Cr_2O_3
SiO_2
TiO_2
10 µm

Figure 9

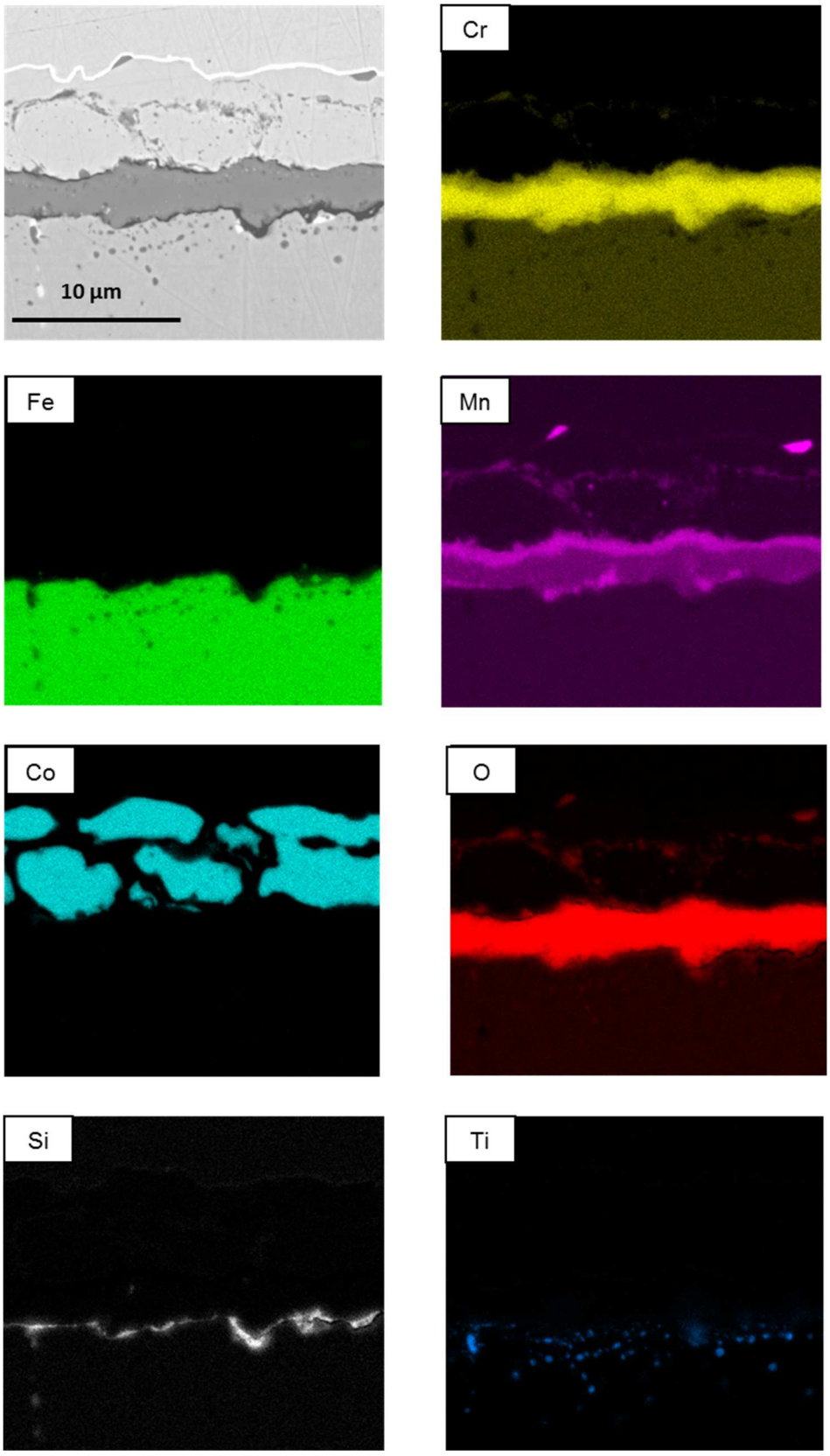

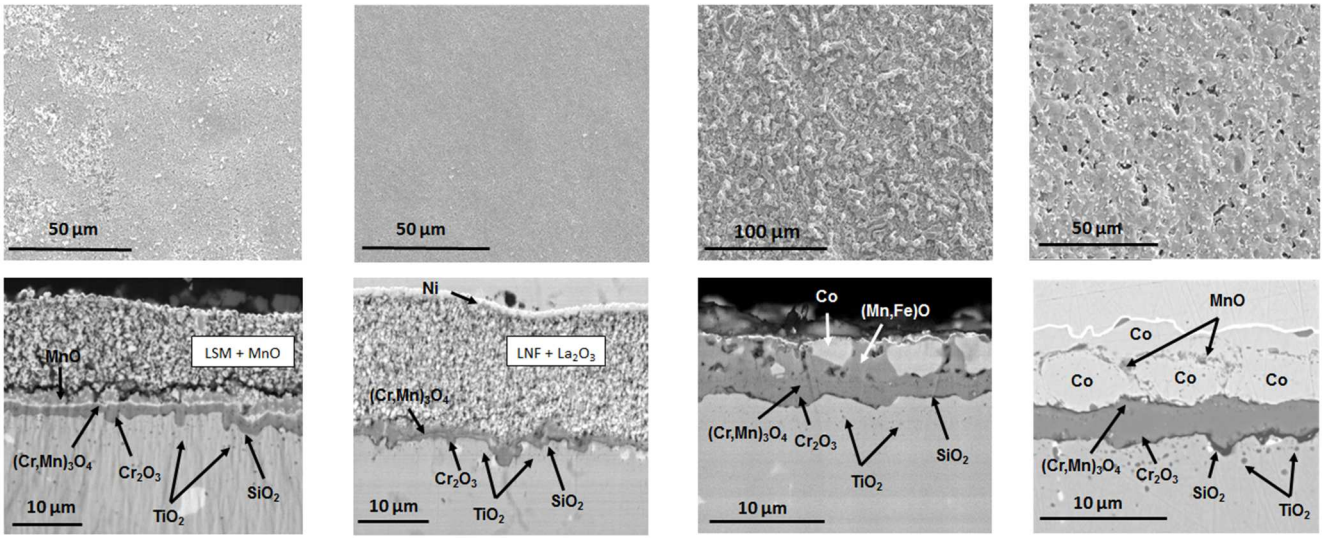
50 µm
50 µm
100 µm
50 µm
MnO
LSM + MnO
(Cr,Mn)3O4
Cr2O3
TiO2
SiO2
10 µm
Ni
LNF + La2O3
(Cr,Mn)3O4
Cr2O3
TiO2
SiO2
10 µm
Co
(Mn,Fe)O
(Cr,Mn)3O4
Cr2O3
TiO2
SiO2
10 µm
MnO
Co
Co
Co
Co
(Cr,Mn)3O4
Cr2O3
SiO2
TiO2
10 µm